

Residual Decoding: Mitigating Hallucinations in Large Vision-Language Models via History-Aware Residual Guidance

Xinrong Chen^{1*} Xu Chu^{1*} Yingmin Qiu² Hengyuan Zhang^{3†} Jing Xiong³ Shiyu Tang⁴ Shuai Liu⁴ Shaokang Yang⁴ Cheng Yang⁴ Hayden Kwok-Hay So³ Ngai Wong^{3†}

¹Peking University ²Beijing University of Posts and Telecommunications

³University of Hong Kong ⁴ByteDance Inc.

chenxinrong23@stu.pku.edu.cn chuxu@stu.pku.edu.cn

Abstract

Large Vision-Language Models (LVLMs) can reason effectively from image-text inputs and perform well in various multimodal tasks. Despite this success, they are affected by language priors and often produce hallucinations. Hallucinations denote generated content that is grammatically and syntactically coherent, yet bears no match or direct relevance to actual visual input. To address this problem, we propose Residual Decoding (ResDec). It is a novel training-free method that uses historical information to aid decoding. The method relies on the internal implicit reasoning mechanism and token logits evolution mechanism of LVLMs to correct biases. Extensive experiments demonstrate that ResDec effectively suppresses hallucinations induced by language priors, significantly improves visual grounding, and reduces object hallucinations. In addition to mitigating hallucinations, ResDec also performs exceptionally well on comprehensive LVLM benchmarks, highlighting its broad applicability.

1. Introduction

Large Vision-Language Models (LVLMs) [3, 5, 12, 17, 39, 52, 66] have become a core component of modern artificial intelligence, playing a crucial role in various vision-language tasks by seamlessly combining visual perception and language understanding. Despite significant progress in recent years, LVLMs are plagued by hallucinations [8, 19, 22, 30, 37, 63], which impede their reliability and applicability in tasks.

Hallucinations in LVLMs can be defined as generating content that is irrelevant to or contradicts the facts in the image [13]. Many studies show that LVLMs hallucinate for three main reasons: statistical pre-training bias [1, 2, 32],

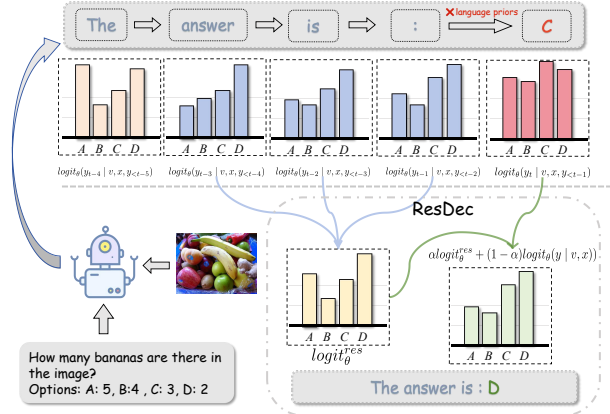


Figure 1. An overview of Residual Decoding. The figure illustrates the Language-Prior Hallucination by focusing on candidate tokens (i.e. A, B, C, and D), and indicates that Residual Decoding with residual guidance effectively mitigates such hallucinations.

weak vision-language alignment [61, 65, 67], and optimization bias [11, 15, 36]. In addition, accumulated language priors [9, 13, 33, 64] during generation further exacerbate these hallucinations. That is, when the model generates responses, textual content gradually fades the visual context, leading to grammatically coherent but visually ungrounded content. This phenomenon can be termed Language-Prior Hallucination.

Researchers have explored various approaches to mitigate Language-Prior Hallucination in LVLMs. Training-based methods include data debiasing [45, 51, 59], modality alignment enhancement [24, 24, 60], and preference alignment [45, 56, 57]. However, these methods require additional training and costly annotations, which limit their scalability in practice. Another line of research focuses on training-free methods, aiming to alleviate hallucinations in a cost-effective manner. For example, recent studies propose contrastive decoding strategies [4, 27, 55] that contrast model outputs under perturbed visual or textual condi-

* Equal contribution.

† Corresponding author.

tions to suppress language priors. Other studies intervene within the model architecture, such as in attention mechanisms [21, 40, 54], feed-forward networks (FFNs) [68], or at the layer level [10, 20, 34], to enhance visual perception and reduce hallucinations in LVLMs. Despite their effectiveness, these training-free methods still have notable limitations: (i) they require $2\times$ or even more inference time and incur higher GPU memory overhead. (ii) they modify internal components of the model, making them less efficient, less concise, and potentially less generalizable. To develop a simple, efficient, and highly generalizable method for mitigating Language-Prior Hallucination, a feasible solution is to design a decoding strategy that is less susceptible to language priors. To achieve this, we revisit the decoding process of LVLMs and find that **signals of the correct answer are already embedded in the logit distributions of preceding tokens before the model explicitly decodes the answer**. As shown in Fig.1, when the model sequentially generates guiding tokens such as “The”, “answer”, “is”, the logits of the correct answer token “D” are already at relatively high values in the logits of these historical tokens. However, when generating the token “:”, the model assigns an abnormally high logits value to the hallucinated token “C”, causing its probability score to surpass that of the genuine token “D”. Ultimately, when the model explicitly decodes the answer, it outputs the incorrect “C”. This observation reveals the essential mechanism of hallucinations in LVLMs: **hallucinated tokens erroneously emerge in the logit distribution at certain moments, and their probabilities gradually approach or even exceed those of genuine tokens**, thereby causing the model to produce hallucinations during final decoding.

To address this issue, we propose **Residual Decoding (ResDec)**, a training-free and plug-and-play decoding strategy. *ResDec* first utilizes Jensen–Shannon Divergence (JSD) to analyze the logits of historical tokens within a time window and discovers a U-shaped pattern (see § 3.2). On the left side of the JSD valley, the distribution transitions from “chaotic” to “convergent”. Near the valley, the distribution becomes smooth and the JSD between adjacent time steps is small, the distribution becomes smooth and the JSD between adjacent time steps is small, indicating a stable logits distribution. This stability suggests that semantics have largely converged and predictions are less influenced by language priors. On the right side of the valley, the distribution diverges again as expressions become divergent. Accordingly, *ResDec* selects logits from the post-convergence region (i.e., near and to the right of the JSD valley), since time steps in this region have stable semantics and exert a substantial effect on the output distribution. These selected logits are then aggregated with confidence weights, yielding a residual guidance that is fused into the decoding logits to reduce Language-Prior Hallucination. *ResDec* re-

quires only a single forward pass, without any contrastive model or external encoder, and incurs nearly the same inference cost as standard decoding. Extensive experiments on multiple LVLM hallucination benchmarks demonstrate that *ResDec* achieves state-of-the-art performance in reducing model hallucinations. Our contributions can be summarized as follows:

- We discover that the essence of hallucinations in LVLMs is that hallucinated tokens emerge in the logits during the decoding stage and surpass genuine tokens (see Fig.1).
- We propose **Residual Decoding (ResDec)**, an efficient, training-free decoding strategy that incurs negligible inference cost for mitigating hallucinations. *ResDec* uses JSD to analyze the logit distributions of historical tokens, aggregates logits from semantically clear tokens to form a residual stream, and merges it into the logits of the decoded token, suppressing Language-Prior Hallucination.
- Extensive experiments reveal that *ResDec* reduces hallucinations in LVLMs and yields improvements on comprehensive datasets, highlighting its broad generalization capability. For instance, *ResDec* achieves an average improvement of 7.84% in accuracy and 8.01% in F1 over the “Regular” decoding strategy across three LVLMs.

2. Related Work

2.1. Causes of Hallucinations in LVLMs

Hallucination [8, 19, 22, 30, 37, 45, 45, 60, 63] has long been a major challenge in Large Vision-Language Models (LVLMs). Recent studies attribute this phenomenon to various factors, such as statistical pre-training bias [23, 32, 46], weak vision–language alignment [24, 24, 60], and optimization objectives [57] that favor linguistic coherence over factual grounding. Notably, *language priors* [9, 13, 33, 64] that further exacerbate hallucinations induced by the aforementioned factors have emerged as the most precisely defined and extensively studied cause. Several studies demonstrate that generative VLMs can, in some cases, completely ignore visual inputs while still outperforming previous approaches, highlighting the dominant influence of language priors [24, 35, 62]. Likewise, Lee et al. [26] introduces a benchmark specifically designed to quantify the extent to which models rely on language priors independent of visual evidence. These studies show that language priors can bias LVLMs towards generating linguistically plausible but visually ungrounded outputs, leading to hallucinations.

2.2. Mitigating Language-Prior Hallucination

To address hallucinations driven by language priors in LVLMs, Wang et al. [55] contrasted output distributions under varied prompts to reduce hallucinated tokens. Moreover, Min et al. [43] encouraged the model to prioritize image input by progressively condensing textual context,

thereby reducing reliance on linguistic patterns. Wan et al. [54] proposes modifying attention weights to mitigate the impact of textual biases and enhance visual grounding. Yang et al. [57] employed on-policy human preference data with Direct Preference Optimization (DPO) to refine the generation strategy, reducing the influence of language priors and improving visual grounding. However, these methods face inherent limitations, including additional computational costs, dependence on extra fine-tuning data, and the need for architectural interventions, which compromises their simplicity, efficiency, and generalizability. Against this backdrop, we propose *ResDec*, a residual decoding strategy tailored to mitigate Language-Prior Hallucination while addressing the aforementioned limitations.

3. Methodology

3.1. Problem Formulation

LVLM Decoding. Consider an LVLM parameterized by θ , with a general architecture consisting of a vision encoder, a vision–language connector, and a Large Language Model (LLM). Given an image v and query x , the LVLM first encodes v into visual tokens using the vision encoder, and then concatenates them with the text tokens from x . The combined sequence is then fed into the LLM to generate the output sequence y autoregressively:

$$y_t \sim p_\theta(y_t | v, x, y_{<t}) = \text{softmax}(\text{logit}_\theta(y_t | v, x, y_{<t})), \quad (1)$$

where y_t denotes the t -th generated token, $y_{<t}$ is the sequence of previously generated tokens, p_θ represents the conditional probability distribution parameterized by the LVLM, and logit_θ denotes the logit distribution.

Language Prior. Taking the mathematical interpretation from Lin et al. [35], we view the *language prior* as the text-only, vision-agnostic conditional distribution $P(y | x)$, i.e., the distribution over outputs y given the textual context x when the visual input v is removed. By considering two equivalent factorizations of $P(y, v | x)$ and applying Bayes rule, one can show that the *language prior* can be “divided out” from the visually conditioned prediction:

$$\frac{P(y | v, x)}{P(y | x)} = \frac{P(v | y, x)}{P(v | x)}. \quad (2)$$

This ratio is analogous to pointwise mutual information (PMI [48]) and captures how the image v supports an output y beyond the language prior. To further make the language prior explicit, it can be expressed as a marginalization over the visual variable and approximated via Monte Carlo [50]:

$$P(y | x) = \mathbb{E}_{v \sim P(v|x)}[P(y | v, x)] \approx \frac{1}{n} \sum_{j=1}^n P(y | v_j, x), \quad (3)$$

where $\{v_j\}_{j=1}^n$ are samples from the image distribution conditioned on x . We adopt this probabilistic view and provide the full derivation in Appendix B.1.

3.2. Implicit Inference of LVLMs

Recent research reveals that LLMs possess implicit multi-token prediction capabilities [44, 49], which means the model already “knows” part of its future outputs before actual decoding. Specifically, as illustrated in Fig. 1, the high-ranking token candidates in the logits at time step t are already implicitly contained in the logits generated during the production of the previous token sequence from y_{t-4} to y_{t-1} . This phenomenon provides a potential avenue for mitigating Language-Prior Hallucination in LVLMs, namely by analyzing the high-ranking tokens in the logits of $y_{<t}$ to help decode correct content at time step t . To further understand this phenomenon and achieve the goal of mitigating hallucinations, we propose two questions:

- **RQ1:** As the input context evolves, can the LVLM progressively and implicitly represent the answer?
- **RQ2:** How do the high-ranking candidate tokens at timestep t change in the logits at timestep $< t$?

Impact of Context Evolution on Implicit Inference (RQ1). As shown in Fig. 2, we observe that as the input context evolves, especially as the question is gradually described completely, the LVLM’s forward-looking perception of the correct reasoning trajectory is progressively activated, manifested as an increase in prediction accuracy and reaching a peak near the token to be decoded (i.e., near the right end of the coordinate axis). This indicates that when the question approaches complete description, the model’s logits already implicitly represent the answer. However, we observe that implicit representation is not always stable. We attribute this to the fact that during the step-by-step token generation process, the LVLM gradually accumulates two different types of biases. Specifically, 1) *Natural language grammar preferences* require the decoded content to satisfy grammar, word order, and punctuation from the pre-training phase. 2) *Task-specific template preferences* require the decoded content to satisfy dialogue templates from the instruction fine-tuning phase (e.g., response templates such as “The answer is :”). This causes the logits of implicit inference to contain not only the answer but also to be affected by other noise. To leverage implicit inference for hallucination mitigation, it is necessary to identify stable implicit representation phases.

Temporal Evolution of Candidate Tokens (RQ2). In this section, our core focus is to explore the fine-grained temporal evolution patterns of the probability distributions of candidate tokens (including genuine tokens and hallucinated tokens). We first define the targeted candidate token set Ω , which consists of the top- k tokens with the highest probabilities at a given time step t . Then, we use a sliding histori-

cal window \mathcal{W} to limit temporal scope for focused analysis. Within this window, we calculate the Jensen–Shannon Divergence (JSD [6]) between the probability distributions of Ω at each adjacent pair of time steps:

$$\text{JSD}(P_{t_1} \parallel P_{t_2}) = \frac{1}{2} D_{\text{KL}}(P_{t_1} \parallel M) + \frac{1}{2} D_{\text{KL}}(P_{t_2} \parallel M), \quad (4)$$

where $M = \frac{1}{2}(P_{t_1} + P_{t_2})$ and D_{KL} denotes the Kullback–Leibler (KL) divergence [25]. Specifically, we compute the JSD curves by averaging over 200 randomly sampled examples from POPE-MSCOCO. As shown in Fig. 3, we observe that JSD values exhibit a U-shaped trend over time. Taking the minimum point of the U-shape as the boundary, the temporal evolution of the candidate token distribution can be decomposed into three phases:

- **(Phase-1) Pre-Semantic Clarity Phase (PSAP):** From the onset to the bottom of the U-shape, JSD exhibits a fluctuating downward trend. We interpret this as indicating that the candidate token distribution is transitioning from an initial state of “disorder” to a state of “convergence”. The minor oscillations in JSD within this phase reflect temporary uncertainty in semantic anchoring, as the model iteratively narrows down its candidate token choices while still navigating potential ambiguities before settling on the core semantics.
- **(Phase-2) Semantic Anchoring Phase (SAP):** At the bottom of the U-shape, JSD approaches 0. This near-zero JSD indicates that the candidate token distribution stabilizes to its highest degree, with minimal divergence between consecutive time steps, reflecting the LVLM’s firm anchoring to core semantics.
- **Expressive Divergence Phase (EDP):** From the bottom of the U-shape to time step t , JSD shows an upward trend, as the LVLM strives to align with the contextual template and pursues diverse expressive forms for candidate tokens. Notably, this phase is susceptible to language priors, as the pursuit of varied expressions may increase reliance on linguistic patterns, causing deviations from visual or factual semantics.

PSAP clearly belongs to an unstable representation phase. Compared to **SAP**, **EDP** appears less stable, it still potentially contains effective decoding guidance due to its incorporation of diverse expressions. Based on the above observations and analyses, we propose *ResDec*, which guides token selection through historical information aggregation, thereby stabilizing the decoding process.

3.3. Residual Decoding

In this section, we present the two key components of *ResDec* strategy: 1) Confidence-weighted aggregation of historical information, discussed in § 3.3.1; and 2) Integration of historical and current information, elaborated in § 3.3.2.

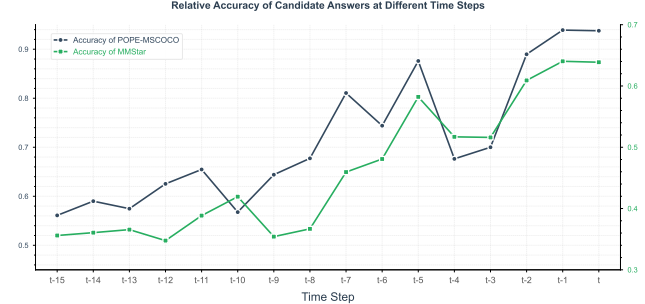


Figure 2. Accuracy of candidate answers at different time steps based on Qwen2.5-VL (7B) in MME and POPE. In both datasets, the candidate answers are binary Yes/No decisions.

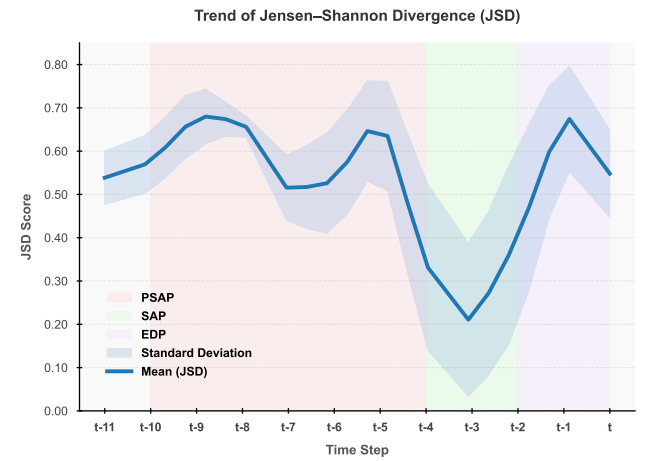


Figure 3. The trend of Jensen–Shannon Divergence (JSD) on 200 randomly sampled POPE-MSCOCO examples using Qwen2.5-VL-Instruct (7B). JSD exhibits a distinct U-shape over time, which we divide into three phases: **PSAP**, **SAP**, and **EDP**.

3.3.1. Historical Information Aggregation

Historical Information Aggregation is a core component of *ResDec*, with the primary goal of dynamically capturing and reusing historical contextual information from the decoding process, which aims to provide sustained and valid references for subsequent token selection.

Historical Aggregation Window. As demonstrated in § 3.2, meaningful historical windows often reside in **SAP** and **EDP** phases. To obtain this window, we typically need to retrieve the corresponding steps from the Semantic Anchoring Phase. This requires empirically setting a predefined historical window W , which will be discussed in Appendix C, and then selecting the high-rank tokens at the current time step t as Candidate Token Pool Ω_t :

$$\Omega_t = \{y_t \mid y_t \in \text{top-}k(\text{logit}_\theta(y_t \mid v, x, y_{<t}), K)\}, \quad (5)$$

Given that **SAP** and **EDP** are phases where semantics have been confirmed and both influence output logits, we weigh

their contributions based on the confidence metric defined in Eq. 6 when aggregating historical information. We then compute the JSD in Eq. 4 between each pair of time steps within the historical window W , and use **SAP** and **EDP** as semi-U-shaped Historical Aggregation Window Δ_t .

Confidence-Weighted Aggregation. While we acknowledge that the historical information within the Historical Aggregation Window is correlated with the current time step, the degree of correlation between information from different historical positions (i.e. time steps) and the current step varies. Motivated by Fu et al. [16], we employ the confidence C_i (for a time step i within the historical window Δ_t), which is formulated as:

$$C_i = -\frac{1}{|\Omega_t|} \sum_{j=1}^{|\Omega_t|} \log P_i(j), \quad (6)$$

where $P_i(j)$ represents the probability of the j -th token in Ω_t . The confidence C_i is a token-level local confidence metric derived from the model’s internal token distribution, and high C_i aligns with low entropy of the token distribution within Ω_t , which denotes the degree of certainty for historical time step i . Based on the mechanisms discussed above, we can obtain the historical residual signal:

$$\text{logit}_\theta^{\text{res}}(y_t | T_{<t-1}) = \sum_{i \in \Delta_t} \left(\frac{C_i}{\sum_{j=1}^n C_j} \cdot \text{logit}_\theta(\hat{y}_i | T_{<i}) \right) \quad (7)$$

where $\hat{y}_i \in \Omega_t$, and $T_{<(\cdot)}$ represents the input to the decoder up to the time step $t-1$. For the first generated token, we use the corresponding token generated from the query x as its historical information:

$$T_{<i} = \begin{cases} \text{concat}(T_v, T_x, y_{<i}) & \text{if } i > 0, \\ \text{concat}(T_v, T_{x < i}) & \text{if } i \leq 0, \end{cases} \quad (8)$$

where T_v represents the encoded visual features and T_x denotes the encoded query text features. In short, for tokens generated in the early stages of generation, where sufficient complete historical information is lacking. We use the decoded tokens corresponding to $T_{x < i}$ in Eq. 8 to serve as the historical interval for these early tokens.

3.3.2. Assembly of History and Present

While the validity of the historical residual signal has been confirmed, exclusive reliance on it in decoding often gives rise to temporal disconnection and contextual fragmentation. Thus, we need to integrate the current temporal information with the historical residual signal. This strategy can be formulated as follows:

$$\begin{aligned} p_{\text{ResDec}}(y_t | v, x, y_{<t}) = & \text{Softmax}[(1 - \alpha) \text{logit}_\theta(y_t | T_{<t-1}) \\ & + \alpha \text{logit}_\theta^{\text{res}}(y_t | T_{<t-1})] \end{aligned} \quad (9)$$

where $\alpha \in [0, 1]$ is a weight balancing the two logit streams. ($\alpha = 0$ reduces to regular decoding). A larger α amplifies the influence of the historical residual signal $\text{logit}_\theta^{\text{res}}$, strengthening anchoring to context and reducing the risk of hallucination. Drawing on previous studies [10, 27, 29], calibrating the entire distribution tends to penalize valid outputs of the original distribution while promoting implausible outputs derived from the augmented distribution.

$$\begin{aligned} \mathcal{V}_{\text{head}}(y_{<t}) = & \{y_t \in \mathcal{V} : \\ & p_\theta(y_t | v, x, y_{<t}) \geq \beta \max_w p_\theta(w | v, x, y_{<t})\} \end{aligned} \quad (10)$$

where \mathcal{V} is the output vocabulary of LVLMs and $\beta \in [0, 1]$ is a hyperparameter for regulating the truncation of the distribution of the next token. Finally, we only consider tokens within $\mathcal{V}_{\text{head}}(y_{<t})$; for those not in $\mathcal{V}_{\text{head}}(y_{<t})$, we set their logits to $-\infty$ to effectively filter them out.

4. Experiments

4.1. Experiment Setup

Benchmarks. To rigorously assess the effectiveness of our *ResDec*, we conduct extensive experiments on eleven benchmarks: POPE [31], CHAIR [47], HallusionBench [18], MME [14], MMBench [41], MMVP [53], ScienceQA [42], MMStar [7], MM-Vet [58], SEEDBench2_Plus [28], LLaVA-Bench (In-the-Wild) [38]. More details can be found in Appendix A.1.

Evaluated LVLMs and Baselines. We assess the effectiveness of our *ResDec* strategy on three contemporary LVLMs: LLaVA-1.5 (7B) [39], Qwen2.5-VL-Instruct (7B) [5], and InstructBLIP (Vicuna-7B) [12], and compare its performance with several state-of-the-art methods, including VCD [27], ICD [55], DoLa [10], OPERA [21], AGLA [4], ONLY [54], MemVR [68], and VISTA [34]. Throughout our experiments, we set $\alpha = 0.5$ and $\beta = 0.1$ for *ResDec*, unless explicitly stated otherwise. More implementation details are provided in Appendix A.

4.2. Performance on Hallucination Benchmarks

Experiments on POPE. Table 1 shows experimental results on the three POPE dataset with LLaVA-1.5, InstructBLIP and Qwen2.5-VL. *ResDec* consistently outperforms the “Regular” decoding strategy by substantial margins (average improvements of 7.84% in accuracy and 8.01% in F1 score) across three LVLMs and settings. Additionally, *ResDec* clearly outperforms all compared SOTA methods, demonstrating its effectiveness in hallucination mitigation.

Experiments on HallusionBench and CHAIR. As shown in Table 2, *ResDec* surpasses regular decoding and other methods across all models on HallusionBench, delivering state-of-the-art performance with consistent gains across metrics. We further assess open-ended captioning on

Models	Methods	Random		Popular		Adversarial		Average	
		Accuracy \uparrow	F1 \uparrow						
LLaVA-1.5	Regular	83.49	82.28	79.98	79.34	76.03	76.26	79.83	79.29
	VCD [27]	86.84	86.83	82.65	83.37	77.31	79.28	82.27	83.16
	ICD [55]	85.11	84.18	81.08	80.74	78.16	78.63	81.45	81.18
	DoLa [10]	84.78	84.19	79.75	80.61	76.32	76.16	80.28	80.32
	OPERA [21]	87.53	86.45	84.21	83.50	80.88	80.69	84.21	83.55
	ONLY [54]	87.49	88.02	79.68	82.27	72.44	77.49	79.87	82.60
	AGLA [4]	88.54	87.71	85.14	84.68	81.13	81.36	84.58	83.13
	MemVR [68]	89.73	89.16	86.35	86.14	82.31	83.97	86.13	86.04
	VISTA [34]	89.64	89.03	85.97	85.87	82.84	82.81	86.15	86.29
	<i>ResDec</i> (ours)	90.21	89.87	86.97	87.22	84.50	83.69	87.23	86.93
InstructBLIP	Regular	80.42	80.94	76.09	77.65	72.37	75.42	76.29	78.00
	VCD [27]	84.11	84.13	79.94	80.80	76.32	78.08	80.12	81.00
	ICD [55]	82.37	83.32	78.13	79.12	75.12	76.24	78.54	79.56
	DoLa [10]	83.00	83.00	78.99	79.85	74.67	76.68	78.89	79.84
	OPERA [21]	85.07	84.39	78.33	80.20	75.50	78.17	79.63	80.92
	ONLY [54]	87.18	88.15	80.43	82.07	74.83	78.00	80.81	82.74
	AGLA [4]	87.30	87.07	81.86	82.58	77.29	79.16	82.15	82.94
	VISTA [34]	87.45	87.66	81.34	80.94	80.82	79.67	83.20	82.76
	<i>ResDec</i> (ours)	88.32	89.11	82.01	83.42	80.41	81.87	83.58	84.80
Qwen2.5-VL	Regular	87.39	86.31	86.03	84.56	84.90	83.35	86.11	84.74
	VCD [27]	88.67	88.21	87.84	85.78	85.45	85.97	87.32	86.65
	ICD [55]	88.67	88.21	87.84	85.78	85.45	85.97	87.32	86.65
	DoLa [10]	87.98	87.71	87.01	85.28	85.67	84.88	86.89	85.96
	OPERA [21]	89.97	90.32	88.89	87.05	86.79	87.35	88.55	88.24
	ONLY [54]	90.94	90.62	89.23	88.21	87.32	86.63	89.16	88.49
	VISTA [34]	90.53	90.77	87.92	88.95	88.03	87.24	88.83	88.99
	<i>ResDec</i> (ours)	91.17	91.62	90.34	89.83	88.96	87.24	90.16	89.56

Table 1. Experimental results on the three POPE subsets with LLaVA-1.5, InstructBLIP and Qwen2.5-VL. The best performances in each setting are highlighted in **bold**.

Models	Methods	HallusionBench			CHAIR	
		fACC \uparrow	qACC \uparrow	aACC \uparrow	CHAIR _S \downarrow	CHAIR _I \downarrow
LLaVA-1.5	Regular	17.9	8.1	41.5	55.0	16.3
	OPERA [21]	16.2	5.5	41.2	47.8	14.6
	ICD [55]	13.9	8.4	38.2	56.2	16.3
	VCD [27]	13.9	11.4	41.1	54.4	16.6
	DoLa [10]	15.7	9.3	41.5	57.0	15.9
	AGLA [4]	17.2	8.3	42.9	43.3	14.1
	ONLY [54]	17.5	9.3	42.7	49.8	14.3
	MemVR [68]	17.9	9.0	42.5	46.6	13.0
	<i>ResDec</i> (ours)	18.2	12.7	45.1	42.7	12.6
InstructBLIP	Regular	10.1	9.5	45.3	54.0	18.1
	OPERA [21]	9.7	8.2	42.3	53.7	12.8
	ICD [55]	7.2	7.5	41.0	59.3	17.5
	VCD [27]	8.1	8.5	43.3	57.0	17.0
	DoLa [10]	8.4	8.6	43.8	60.0	20.1
	AGLA [4]	9.7	9.2	45.9	49.0	12.1
Qwen2.5-VL	<i>ResDec</i> (ours)	11.3	10.2	46.5	47.7	11.3
	Regular	43.4	45.8	69.1	30.6	8.4
	OPERA [21]	41.5	43.4	68.7	28.4	7.6
	ICD [55]	38.7	39.8	67.6	30.9	8.3
	VCD [27]	39.8	41.3	68.7	27.9	7.8
	DoLa [10]	40.8	39.5	66.9	28.2	8.9
	<i>ResDec</i> (ours)	47.1	49.0	71.6	25.8	6.8

Table 2. HallusionBench and CHAIR evaluation results of different methods. We limit the maximum number of new tokens 128. Lower (\downarrow) CHAIR_S and CHAIR_I denote better performance. The best performances in each setting are highlighted in **bold**.

CHAIR; relative to regular decoding, *ResDec* yields average improvements of 16.57% on CHAIR_S and 26.44% on CHAIR_I with significant enhancements across InstructBLIP, LLaVA-1.5 and Qwen2.5-VL. Collectively, these results indicate that *ResDec* effectively mitigates hallucinations while enhancing open-ended caption generation, high-

lighting its versatility and robust overall performance.

4.3. Performance on Comprehensive Benchmarks

We evaluate the performance of *ResDec* on comprehensive benchmarks, including MM-Vet, MME, MMBench, MMVP, MMStar, and SEEDBench2_Plus. As shown in Table 3, *ResDec* consistently outperforms competing methods across LLaVA-1.5, InstructBLIP, and Qwen2.5-VL, demonstrating its robust generalizability. For example, *ResDec* outperforms “Regular” decoding by 2.87%, 2.99%, and 11.65% on MME, ScienceQA, and MMVP, respectively, across three models. This consistency across different LVLMs and benchmarks highlights the effectiveness of *ResDec* in mitigating hallucinations and enhancing multimodal reasoning, aligning visual and linguistic information at both object and attribute levels.

4.4. Ablation Study

Size of Candidate Token Pool. In the paragraph, we explore the size of Candidate Token Pool $|\Omega_t|$ to observe its impact on *ResDec*. To determine the optimal size of the candidate token pool, we explore sizes ranging from 2 to 4096. The results shown in Fig. 4 indicate that the most suitable size for the Candidate Token Pool, denoted as Ω_t , falls between 64 and 512 tokens. Both excessively small and

Models	Methods	MME \uparrow	MMBench \uparrow	ScienceQA \uparrow	MMVP \uparrow	MMStar \uparrow	MM-Vet \uparrow	SEEDBench2_Plus \uparrow	LLaVA-Bench \uparrow
LLaVA-1.5	Regular	1810.41	64.24	68.02	20.67	32.67	31.10	38.65	61.80
	VCD [27]	1818.67	55.14	62.96	20.33	29.20	30.20	39.31	58.50
	ICD [55]	1757.28	39.03	51.61	17.00	25.80	26.30	35.40	55.10
	DoLa [10]	1829.72	63.78	68.32	20.67	31.67	30.70	38.21	60.70
	OPERA [21]	1844.51	64.32	68.77	21.00	33.00	32.00	39.75	61.40
	ONLY [54]	1876.35	64.87	67.23	21.33	32.27	32.50	37.90	61.60
	MemVR [68]	1864.68	65.12	68.96	23.67	32.73	32.80	40.84	62.20
	VISTA [34]	1857.64	65.00	68.22	20.33	32.60	32.00	40.49	60.90
InstructBLIP	ResDec (ours)	1881.57	65.70	69.46	24.00	33.40	33.20	41.15	62.60
	Regular	1385.25	38.32	60.49	17.33	32.20	33.10	30.87	59.80
	VCD [27]	1408.15	29.13	56.42	18.00	31.67	29.30	28.55	61.10
	ICD [55]	1375.48	21.28	49.78	15.00	24.20	23.60	26.39	51.00
	DoLa [10]	1398.95	38.81	58.21	17.33	31.27	32.50	30.61	56.60
	OPERA [21]	1406.54	39.31	60.83	17.67	30.67	33.70	31.80	63.10
	VISTA [34]	1413.05	39.73	60.93	18.33	32.40	33.80	32.02	63.50
	ResDec (ours)	1426.83	40.13	62.92	19.00	32.67	34.30	33.38	64.40
Qwen2.5-VL	Regular	2309.42	81.05	88.99	58.00	63.87	67.10	69.61	91.00
	VCD [27]	2296.78	69.23	90.08	59.67	63.60	64.70	67.90	89.50
	ICD [55]	2284.41	60.06	84.83	55.33	57.20	57.70	62.32	83.70
	DoLa [10]	2313.23	79.03	88.75	59.33	64.20	65.60	67.19	87.30
	OPERA [21]	2318.13	81.87	90.33	61.67	64.53	66.90	68.99	91.30
	VISTA [34]	2324.93	81.04	90.23	60.33	64.27	67.80	69.30	91.70
	ResDec (ours)	2348.40	82.64	90.48	63.33	65.47	68.70	70.31	91.90

Table 3. Experimental results on the eight comprehensive benchmarks with LLaVA-1.5, InstructBLIP and Qwen2.5-VL. The best performances in each setting are highlighted in **bold**.

α	β	MME			POPE		MMStar	
		Accuracy \uparrow	Accuracy \uparrow	F1 \uparrow	Accuracy \uparrow	F1 \uparrow	Accuracy \uparrow	Accuracy \uparrow
0.25	0.1	2326.31	89.64	89.11	64.20			
0.5	0.1	2348.40	90.16	89.56	65.40			
0.75	0.1	1875.31	82.56	81.93	62.67			
1.0	0.1	1583.17	72.50	71.73	61.80			
0.5	0	2221.73	87.21	87.73	64.20			
0.5	0.001	2184.91	88.02	87.21	63.47			
0.5	0.01	2274.15	88.74	88.27	64.80			
0.5	0.2	2348.40	90.35	89.96	65.67			
0.5	0.5	2353.21	89.83	89.51	66.07			

Table 4. An ablation study of α and β in Qwen2.5-VL on MME, POPE and MMStar benchmarks. The best performance in each setting is emphasized in **boldface**.

large sizes lead to inaccurate localization of **SAP**, which in turn causes performance degradation. This trend can be explained as follows: When Ω_t is too small, the pool fails to capture comprehensive variations in JSD, making it insufficient to reflect the critical differences required for accurate **SAP** localization. Conversely, an excessively large Ω_t inadvertently incorporates too much local information from earlier time steps, which distorts the JSD calculation, rendering the divergence metric inaccurate and ultimately undermining the precision of **SAP** localization.

Effect of Hyperparameters in *ResDec*. To investigate the impact of hyperparameters α and β on *ResDec*, we conduct an ablation study on three benchmarks. α modulates the amplification between the historical residual signal and the original output distributions in Eq. 9. The historical signal helps rectify hallucination issues by retaining valid prior information. As shown in Table 4, α performs well below

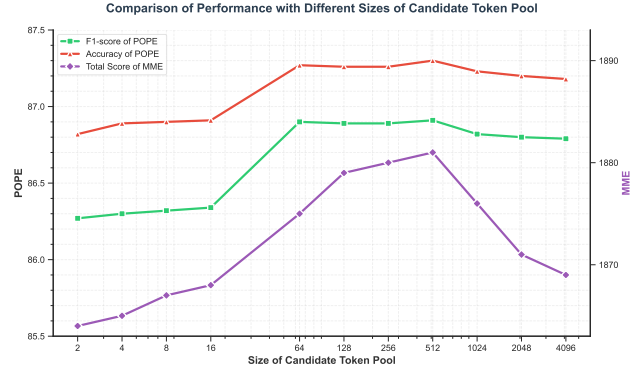


Figure 4. Ablation study on different sizes of Candidate Token Pool conducted on LLaVA-1.5 and focusing on POPE and MME. The optimal size of Candidate Token Pool ranges from 64 to 512, while excessively small or large sizes degrade performance by impairing **SAP** localization.

0.5, but higher values ($\alpha = 0.75, 1.0$) often cause adverse effects, as the historical signal is an auxiliary correction, not directly usable for decoding. Meanwhile, β controls the adaptive plausible constraint in *ResDec*, with larger values indicating more aggressive truncation. Setting $\beta = 0$ leads to suboptimal performance, while $\beta > 0$ improves performance, validating the constraint's effectiveness.

4.5. Analysis

Effect of Different Decoding Strategies. Besides direct sampling, we also present an ablation study with various decoding strategies on the POPE and MME datasets using LLaVA-1.5. The experiment includes three additional de-

[Instruction] Please describe this image in detail.

[Regular Decoding] The image features a large red and white bus driving under a bridge. The bus is positioned in the middle of the scene, occupying a significant portion of the image. The bridge spans across the entire width of the scene, providing a sense of depth to the image. There are **several people visible in the scene**, with one person standing near the left edge of the image, another person closer to the center, and a third person on the right side. Additionally, there is a car parked on the right side of the image, slightly behind the bus.



[Residual Decoding] The image depicts a large red bus parked under a bridge, with a bus stop a short distance away. The bus stop sign is visible, and a sign on the bus advertises a nearby theater show, "Cinderella." The bus is the main focus of the scene, and the theater show and bus stop sign signify the location is a bustling area for public transportation and entertainment.

[Instruction] Please describe this image in detail.

[Regular Decoding] The image depicts a lively scene at a fruit stand where a group of people is gathered around a man selling fruit. The man is standing behind the stand, attending to the customers. The stand is filled with a variety of fruits, including oranges, **apples**, and **bananas**. There are several oranges displayed in different areas of the stand, with some placed closer to the man and others further away. **Apples** can be seen in various spots, with some closer to the man and others further away. **Bananas** are also present, with a few bunches placed on the stand. The customers are engaged in conversation and enjoying their time at the fruit stand. Some of them are holding cups, possibly filled with drinks, while others are carrying handbags.



[Residual Decoding] The image depicts a lively outdoor market scene, where a group of people, predominantly women, are gathered around a fruit and drink stand. The stand sells oranges and soda, and a man, possibly the seller, is attending to the customers. There are several oranges on display, and a variety of bottles and cups can be seen, both on the stand and in the hands of the customers. The people in the market are standing close to the stand, and a handbag is visible in the foreground, near one of the women. The outdoor market is a bustling scene, with the people engaging in conversations and, in some cases, enjoying a drink, while the seller attends to the customers and the fruit and drink stand.

Figure 5. Case study comparing regular decoding and residual decoding in image captioning. Hallucinated details in “regular” decoding outputs are highlighted in red.

Decoding Strategy	POPE			MME
	Accuracy ↑	F1 ↑	Accuracy ↑	
Nucleus Sampling	Vanilla	77.61	78.43	1792.35
	<i>ResDec</i>	84.15	85.82	1846.82
Top-K Sampling	Vanilla	76.62	77.32	1773.67
	<i>ResDec</i>	83.82	84.05	1852.09
Temperature Sampling	Vanilla	79.13	78.56	1803.16
	<i>ResDec</i>	86.62	85.82	1872.91
Greedy	Vanilla	79.83	79.29	1810.41
	<i>ResDec</i>	87.23	86.93	1881.57

Table 5. An ablation study of different decoding strategies. “Vanilla” means sampling from the original distribution.

coding strategies: Nucleus Sampling ($p = 0.7$), Top-K sampling ($k = 50$), Temperature Sampling ($t = 0.5$), and Greedy decoding. The results in Table 5 demonstrate that our *ResDec* consistently mitigates hallucinations, regardless of the adopted decoding strategy. This highlights the robustness of *ResDec* in improving text generation quality and accuracy across different decoding strategies.

Efficiency Comparison. To analyze the performance of *ResDec* in terms of efficiency metrics, we refer to Table 6. *ResDec* needs to maintain a sequence of historical logits during operation. Crucially, by reusing historical logits that are naturally generated as an inherent part of inference, *ResDec* incurs extremely negligible additional latency and memory overhead. Compared with existing SOTA methods for hallucination mitigation, our *ResDec* achieves the lowest latency (only $0.02\times$ slower than Greedy decoding). These results highlight the effective practicality of *ResDec*, which achieves an optimal balance between hallucination mitigation and computational efficiency.

Case Study. Fig. 5 presents two case studies showing how,

Methods	Latency ↓ (ms/token)	Throughput ↑ (token/s)	Memory Cost ↓ (MB)
Greedy	28.54	35.04	14257
OPERA [21]	104.46	9.57	21300
ICD [55]	30.82	32.44	14263
VCD [27]	62.79	15.93	14967
ONLY [54]	30.54	32.75	14951
MemVR [68]	29.68	33.69	14345
VISTA [34]	36.32	27.53	14783
<i>ResDec</i> (ours)	29.11	34.35	14296

Table 6. Performance comparison of SOTA methods and *ResDec* in latency, throughput, and memory usage. The best and suboptimal results are highlighted in **bold** and underlined, respectively.

under the same visual input and prompt, regular decoding tends to introduce hallucinated details not visible in the images, such as *additional people* and *specific fruit types*, based on language priors and pretraining co-occurrence patterns. In contrast, residual decoding reduces these hallucinations while maintaining coherence and visual alignment. More examples and ablation studies are in Appendix D.

5. Conclusion

In this paper, we investigated the root cause of hallucinations in LVLMs and revealed that hallucinated tokens emerge and surpass visually grounded tokens during decoding. Based on this, we introduced Residual Decoding (*ResDec*), a training-free decoding strategy that mitigates hallucinations with negligible inference overhead. *ResDec* leverages the semantic clarity of historical token distributions and integrates residual guidance into decoding, effectively suppressing Language-Prior Hallucination. Extensive experiments on hallucination benchmarks show *ResDec* alleviates hallucinations while preserving descriptive coherence and efficiency. This work offers insights

for decoding-stage interventions in LVLMs and paves the way for more reliable, visually grounded generation.

References

[1] Vedika Agarwal, Rakshith Shetty, and Mario Fritz. Towards causal vqa: Revealing and reducing spurious correlations by invariant and covariant semantic editing, 2020. 1

[2] Aishwarya Agrawal, Dhruv Batra, and Devi Parikh. Analyzing the behavior of visual question answering models. In *Proceedings of the 2016 Conference on Empirical Methods in Natural Language Processing*, pages 1955–1960, Austin, Texas, 2016. Association for Computational Linguistics. 1

[3] Jean-Baptiste Alayrac, Jeff Donahue, Pauline Luc, Antoine Miech, Iain Barr, Yana Hasson, Karel Lenc, Arthur Mensch, Katie Millican, Malcolm Reynolds, Roman Ring, Eliza Rutherford, Serkan Cabi, Tengda Han, Zhitao Gong, Sina Samangoocci, Marianne Monteiro, Jacob Menick, Sebastian Borgeaud, Andrew Brock, Aida Nematzadeh, Sahand Sharifzadeh, Mikolaj Binkowski, Ricardo Barreira, Oriol Vinyals, Andrew Zisserman, and Karen Simonyan. Flamingo: a visual language model for few-shot learning, 2022. 1

[4] Wenbin An, Feng Tian, Sicong Leng, Jiahao Nie, Haonan Lin, QianYing Wang, Ping Chen, Xiaoqin Zhang, and Shijian Lu. Mitigating object hallucinations in large vision-language models with assembly of global and local attention, 2025. 1, 5, 6

[5] Shuai Bai, Keqin Chen, Xuejing Liu, Jialin Wang, Wenbin Ge, Sibo Song, Kai Dang, Peng Wang, Shijie Wang, Jun Tang, Humen Zhong, Yuanzhi Zhu, Mingkun Yang, Zhao-hai Li, Jianqiang Wan, Pengfei Wang, Wei Ding, Zheren Fu, Yiheng Xu, Jiaob Ye, Xi Zhang, Tianbao Xie, Zesen Cheng, Hang Zhang, Zhibo Yang, Haiyang Xu, and Junyang Lin. Qwen2.5-vl technical report, 2025. 1, 5

[6] Jop Briët and Peter Harremoës. Properties of classical and quantum jensen-shannon divergence. *Physical Review A*, 79(5), 2009. 4

[7] Lin Chen, Jinsong Li, Xiaoyi Dong, Pan Zhang, Yuhang Zang, Zehui Chen, Haodong Duan, Jiaqi Wang, Yu Qiao, Dahua Lin, and Feng Zhao. Are we on the right way for evaluating large vision-language models?, 2024. 5, 1

[8] Zhiyuan Chen, Yuecong Min, Jie Zhang, Bei Yan, Jiahao Wang, Xiaozhen Wang, and Shiguang Shan. A survey of multimodal hallucination evaluation and detection, 2025. 1, 2

[9] Xu Chu, Xinrong Chen, Guanyu Wang, Zhijie Tan, Kui Huang, Wenyu Lv, Tong Mo, and Weiping Li. Qwen look again: Guiding vision-language reasoning models to re-attention visual information. *arXiv preprint arXiv:2505.23558*, 2025. 1, 2

[10] Yung-Sung Chuang, Yujia Xie, Hongyin Luo, Yoon Kim, James Glass, and Pengcheng He. Dola: Decoding by contrasting layers improves factuality in large language models. *arXiv preprint arXiv:2309.03883*, 2023. 2, 5, 6, 7

[11] Alberto Compagnoni, Davide Caffagni, Nicholas Moratelli, Lorenzo Baraldi, Marcella Cornia, and Rita Cucchiara. Mitigating hallucinations in multimodal llms via object-aware preference optimization, 2025. 1

[12] Wenliang Dai, Junnan Li, Dongxu Li, Anthony Meng Huat Tiong, Junqi Zhao, Weisheng Wang, Boyang Li, Pascale Fung, and Steven Hoi. Instructclip: Towards general-purpose vision-language models with instruction tuning, 2023. 1, 5

[13] Alessandro Favero, Luca Zancato, Matthew Trager, Siddharth Choudhary, Pramuditha Perera, Alessandro Achille, Ashwin Swaminathan, and Stefano Soatto. Multi-modal hallucination control by visual information grounding. In *Proceedings of the IEEE/CVF Conference on Computer Vision and Pattern Recognition*, pages 14303–14312, 2024. 1, 2

[14] Chaoyou Fu, Peixian Chen, Yunhang Shen, Yulei Qin, Mengdan Zhang, Xu Lin, Jinrui Yang, Xiawu Zheng, Ke Li, Xing Sun, Yunsheng Wu, Rongrong Ji, Caifeng Shan, and Ran He. Mme: A comprehensive evaluation benchmark for multimodal large language models, 2025. 5, 1

[15] Yuhang Fu, Ruobing Xie, Xingwu Sun, Zhanhui Kang, and Xirong Li. Mitigating hallucination in multimodal large language model via hallucination-targeted direct preference optimization, 2024. 1

[16] Yichao Fu, Xuewei Wang, Yuandong Tian, and Jiawei Zhao. Deep think with confidence, 2025. 5

[17] Tao Gong, Chengqi Lyu, Shilong Zhang, Yudong Wang, Miao Zheng, Qian Zhao, Kuikun Liu, Wenwei Zhang, Ping Luo, and Kai Chen. Multimodal-gpt: A vision and language model for dialogue with humans, 2023. 1

[18] Tianrui Guan, Fuxiao Liu, Xiyang Wu, Ruiqi Xian, Zongxia Li, Xiaoyu Liu, Xijun Wang, Lichang Chen, Furong Huang, Yaser Yacoob, et al. Hallusionbench: an advanced diagnostic suite for entangled language hallucination and visual illusion in large vision-language models. In *Proceedings of the IEEE/CVF Conference on Computer Vision and Pattern Recognition*, pages 14375–14385, 2024. 5, 1

[19] Anisha Gunjal, Jihan Yin, and Erhan Bas. Detecting and preventing hallucinations in large vision language models, 2024. 1, 2

[20] Zhihui Guo, Xin Man, Hui Xu, and Jie Shao. Lisa: A layer-wise integration and suppression approach for hallucination mitigation in multimodal large language models, 2025. 2

[21] Qidong Huang, Xiaoyi Dong, Pan Zhang, Bin Wang, Conghui He, Jiaqi Wang, Dahua Lin, Weiming Zhang, and Nenghai Yu. Opera: Alleviating hallucination in multimodal large language models via over-trust penalty and retrospection-allocation, 2024. 2, 5, 6, 7, 8

[22] Wen Huang, Hongbin Liu, Minxin Guo, and Neil Gong. Visual hallucinations of multi-modal large language models. In *Findings of the Association for Computational Linguistics: ACL 2024*, pages 9614–9631, Bangkok, Thailand, 2024. Association for Computational Linguistics. 1, 2

[23] Yiyang Huang, Liang Shi, Yitian Zhang, Yi Xu, and Yun Fu. Shield: Suppressing hallucinations in lvlm encoders via bias and vulnerability defense, 2025. 2

[24] Chaoya Jiang, Haiyang Xu, Mengfan Dong, Jiaxing Chen, Wei Ye, Ming Yan, Qinghao Ye, Ji Zhang, Fei Huang, and Shikun Zhang. Hallucination augmented contrastive learning for multimodal large language model, 2024. 1, 2

[25] Solomon Kullback and Richard A Leibler. On information and sufficiency. *The annals of mathematical statistics*, 22(1):79–86, 1951. 4

[26] Kang-il Lee, Minbeom Kim, Seunghyun Yoon, Minsung Kim, Dongryeol Lee, Hyukhun Koh, and Kyomin Jung. VLind-bench: Measuring language priors in large vision-language models. In *Findings of the Association for Computational Linguistics: NAACL 2025*, pages 4129–4144, Albuquerque, New Mexico, 2025. Association for Computational Linguistics. 2

[27] Sicong Leng, Hang Zhang, Guanzheng Chen, Xin Li, Shijian Lu, Chunyan Miao, and Lidong Bing. Mitigating object hallucinations in large vision-language models through visual contrastive decoding, 2023. 1, 5, 6, 7, 8

[28] Bohao Li, Yuying Ge, Yi Chen, Yixiao Ge, Ruimao Zhang, and Ying Shan. Seed-bench-2-plus: Benchmarking multi-modal large language models with text-rich visual comprehension, 2024. 5, 1

[29] Xiang Lisa Li, Ari Holtzman, Daniel Fried, Percy Liang, Jason Eisner, Tatsunori Hashimoto, Luke Zettlemoyer, and Mike Lewis. Contrastive decoding: Open-ended text generation as optimization, 2023. 5

[30] Yifan Li, Yifan Du, Kun Zhou, Jinpeng Wang, Wayne Xin Zhao, and Ji-Rong Wen. Evaluating object hallucination in large vision-language models, 2023. 1, 2

[31] Yifan Li, Yifan Du, Kun Zhou, Jinpeng Wang, Xin Zhao, and Ji-Rong Wen. Evaluating object hallucination in large vision-language models. In *Proceedings of the 2023 Conference on Empirical Methods in Natural Language Processing*, pages 292–305, Singapore, 2023. Association for Computational Linguistics. 5

[32] Yifan Li, Kun Zhou, Wayne Xin Zhao, Lei Fang, and Ji-Rong Wen. Analyzing and mitigating object hallucination: A training bias perspective, 2025. 1, 2

[33] Zhuowei Li, Haizhou Shi, Yunhe Gao, Di Liu, Zhenting Wang, Yuxiao Chen, Ting Liu, Long Zhao, Hao Wang, and Dimitris N Metaxas. The hidden life of tokens: Reducing hallucination of large vision-language models via visual information steering. *arXiv preprint arXiv:2502.03628*, 2025. 1, 2

[34] Zhuowei Li, Haizhou Shi, Yunhe Gao, Di Liu, Zhenting Wang, Yuxiao Chen, Ting Liu, Long Zhao, Hao Wang, and Dimitris N. Metaxas. The hidden life of tokens: Reducing hallucination of large vision-language models via visual information steering, 2025. 2, 5, 6, 7, 8

[35] Zhiqiu Lin, Xinyue Chen, Deepak Pathak, Pengchuan Zhang, and Deva Ramanan. Revisiting the role of language priors in vision-language models, 2024. 2, 3

[36] Chenxi Liu, Tianyi Xiong, Yanshuo Chen, Ruibo Chen, Yihan Wu, Junfeng Guo, Tianyi Zhou, and Heng Huang. Modality-balancing preference optimization of large multi-modal models by adversarial negative mining, 2025. 1

[37] Fuxiao Liu, Kevin Lin, Linjie Li, Jianfeng Wang, Yaser Yacoob, and Lijuan Wang. Mitigating hallucination in large multi-modal models via robust instruction tuning, 2024. 1, 2

[38] Haotian Liu, Chunyan Li, Qingyang Wu, and Yong Jae Lee. Visual instruction tuning. In *Advances in Neural Information Processing Systems*, pages 34892–34916. Curran Associates, Inc., 2023. 5, 2

[39] Haotian Liu, Chunyan Li, Yuheng Li, and Yong Jae Lee. Improved baselines with visual instruction tuning. In *Proceedings of the IEEE/CVF Conference on Computer Vision and Pattern Recognition (CVPR)*, pages 26296–26306, 2024. 1, 5

[40] Shi Liu, Kecheng Zheng, and Wei Chen. Paying more attention to image: A training-free method for alleviating hallucination in lylms, 2024. 2

[41] Yuan Liu, Haodong Duan, Yuanhan Zhang, Bo Li, Songyang Zhang, Wangbo Zhao, Yike Yuan, Jiaqi Wang, Conghui He, Ziwei Liu, Kai Chen, and Dahua Lin. Mmbench: Is your multi-modal model an all-around player?, 2024. 5, 1

[42] Pan Lu, Swaroop Mishra, Tony Xia, Liang Qiu, Kai-Wei Chang, Song-Chun Zhu, Oyvind Tafjord, Peter Clark, and Ashwin Kalyan. Learn to explain: Multimodal reasoning via thought chains for science question answering, 2022. 5, 1

[43] Kyungmin Min, Minbeom Kim, Kang il Lee, Dongryeol Lee, and Kyomin Jung. Mitigating hallucinations in large vision-language models via summary-guided decoding, 2025. 2

[44] Koyena Pal, Jiuding Sun, Andrew Yuan, Byron Wallace, and David Bau. Future lens: Anticipating subsequent tokens from a single hidden state. In *Proceedings of the 27th Conference on Computational Natural Language Learning (CoNLL)*, pages 548–560, Singapore, 2023. Association for Computational Linguistics. 3

[45] Shangpin Peng, Senqiao Yang, Li Jiang, and Zhuotao Tian. Mitigating object hallucinations via sentence-level early intervention, 2025. 1, 2

[46] Ryan Ramos, Yusuke Hirota, Yuta Nakashima, and Noa Garcia. From global to local: Social bias transfer in clip, 2025. 2

[47] Anna Rohrbach, Lisa Anne Hendricks, Kaylee Burns, Trevor Darrell, and Kate Saenko. Object hallucination in image captioning. In *Proceedings of the 2018 Conference on Empirical Methods in Natural Language Processing*, pages 4035–4045, Brussels, Belgium, 2018. Association for Computational Linguistics. 5, 1

[48] François Role and Mohamed Nadif. Handling the impact of low frequency events on co-occurrence based measures of word similarity-a case study of pointwise mutual information. In *International conference on knowledge discovery and information retrieval*, pages 218–223. Scitepress, 2011. 3

[49] Mohammad Samragh, Arnav Kundu, David Harrison, Kumi Nishu, Devang Naik, Minsik Cho, and Mehrdad Farajtabar. Your llm knows the future: Uncovering its multi-token prediction potential, 2025. 3

[50] Alexander Shapiro. Monte carlo sampling methods. In *Stochastic Programming*, pages 353–425. Elsevier, 2003. 3

[51] Zhiqing Sun, Sheng Shen, Shengcao Cao, Haotian Liu, Chunyan Li, Yikang Shen, Chuang Gan, Liang-Yan Gui, Yu-Xiong Wang, Yiming Yang, Kurt Keutzer, and Trevor Darrell. Aligning large multimodal models with factually augmented rlhf, 2023. 1

[52] V Team, Wenyi Hong, Wenmeng Yu, Xiaotao Gu, Guo Wang, Guobing Gan, Haomiao Tang, Jiale Cheng, Ji Qi, Junhui Ji, Lihang Pan, Shuaiqi Duan, Weihan Wang, Yan Wang, Yean Cheng, Zehai He, Zhe Su, Zhen Yang, Ziyang Pan, Aohan Zeng, Baoxu Wang, Bin Chen, Boyan Shi, Changyu Pang, Chenhui Zhang, Da Yin, Fan Yang, Guoqing Chen, Jiazheng Xu, Jiale Zhu, Jiali Chen, Jing Chen, Jin-hao Chen, Jinghao Lin, Jinjiang Wang, Junjie Chen, Leqi Lei, Letian Gong, Leyi Pan, Mingdao Liu, Mingde Xu, Mingzhi Zhang, Qinkai Zheng, Sheng Yang, Shi Zhong, Shiyu Huang, Shuyuan Zhao, Siyan Xue, Shangqin Tu, Shengbiao Meng, Tianshu Zhang, Tianwei Luo, Tianxiang Hao, Tianyu Tong, Wenkai Li, Wei Jia, Xiao Liu, Xiaohan Zhang, Xin Lyu, Xinyue Fan, Xuancheng Huang, Yanning Wang, Yadong Xue, Yanfeng Wang, Yanzi Wang, Yifan An, Yifan Du, Yiming Shi, Yiheng Huang, Yilin Niu, Yuan Wang, Yuanchang Yue, Yuchen Li, Yutao Zhang, Yuting Wang, Yu Wang, Yuxuan Zhang, Zhao Xue, Zhenyu Hou, Zhengxiao Du, Zihan Wang, Peng Zhang, Debing Liu, Bin Xu, Juanzi Li, Minlie Huang, Yuxiao Dong, and Jie Tang. Glm-4.5v and glm-4.1v-thinking: Towards versatile multimodal reasoning with scalable reinforcement learning, 2025. 1

[53] Shengbang Tong, Zhuang Liu, Yuexiang Zhai, Yi Ma, Yann LeCun, and Saining Xie. Eyes wide shut? exploring the visual shortcomings of multimodal llms, 2024. 5, 1

[54] Zifu Wan, Ce Zhang, Silong Yong, Martin Q. Ma, Simon Stepputtis, Louis-Philippe Morency, Deva Ramanan, Katia Sycara, and Yaqi Xie. Only: One-layer intervention sufficiently mitigates hallucinations in large vision-language models, 2025. 2, 3, 5, 6, 7, 8

[55] Xintong Wang, Jingheng Pan, Liang Ding, and Chris Biemann. Mitigating hallucinations in large vision-language models with instruction contrastive decoding, 2024. 1, 2, 5, 6, 7, 8

[56] Jiulong Wu, Zhengliang Shi, Shuaiqiang Wang, Jizhou Huang, Dawei Yin, Lingyong Yan, Min Cao, and Min Zhang. Mitigating hallucinations in large vision-language models via entity-centric multimodal preference optimization, 2025. 1

[57] Zhihe Yang, Xufang Luo, Dongqi Han, Yunjian Xu, and Dongsheng Li. Mitigating hallucinations in large vision-language models via dpo: On-policy data hold the key, 2025. 1, 2, 3

[58] Weihao Yu, Zhengyuan Yang, Linjie Li, Jianfeng Wang, Kevin Lin, Zicheng Liu, Xinchao Wang, and Lijuan Wang. Mm-vet: Evaluating large multimodal models for integrated capabilities, 2024. 5, 1

[59] Zefeng Zhang, Hengzhu Tang, Jiawei Sheng, Zhenyu Zhang, Yiming Ren, Zhenyang Li, Dawei Yin, Duohe Ma, and Tingwen Liu. Debiasing multimodal large language models via noise-aware preference optimization, 2025. 1

[60] Zongmeng Zhang, Wengang Zhou, Jie Zhao, and Houqiang Li. Robust multimodal large language models against modality conflict, 2025. 1, 2

[61] Linxi Zhao, Yihe Deng, Weitong Zhang, and Quanquan Gu. Mitigating object hallucination in large vision-language models via image-grounded guidance, 2025. 1

[62] Zhiyuan Zhao, Bin Wang, Linke Ouyang, Xiaoyi Dong, Jiaqi Wang, and Conghui He. Beyond hallucinations: Enhancing lmlms through hallucination-aware direct preference optimization, 2024. 2

[63] Kening Zheng, Junkai Chen, Yibo Yan, Xin Zou, Huiyu Zhou, and Xuming Hu. Reefknot: A comprehensive benchmark for relation hallucination evaluation, analysis and mitigation in multimodal large language models. In *Findings of the Association for Computational Linguistics: ACL 2025*, pages 6193–6212, Vienna, Austria, 2025. Association for Computational Linguistics. 1, 2

[64] Yiyang Zhou, Chenhang Cui, Jaehong Yoon, Linjun Zhang, Zhun Deng, Chelsea Finn, Mohit Bansal, and Huaxiu Yao. Analyzing and mitigating object hallucination in large vision-language models. *arXiv preprint arXiv:2310.00754*, 2023. 1, 2

[65] Yiyang Zhou, Zhiyuan Fan, Dongjie Cheng, Sihan Yang, Zhaorun Chen, Chenhang Cui, Xiya Wang, Yun Li, Linjun Zhang, and Huaxiu Yao. Calibrated self-rewarding vision language models, 2024. 1

[66] Jinguo Zhu, Weiyun Wang, Zhe Chen, Zhaoyang Liu, Shenglong Ye, Lixin Gu, Hao Tian, Yuchen Duan, Weijie Su, Jie Shao, Zhangwei Gao, Erfei Cui, Xuehui Wang, Yue Cao, Yangzhou Liu, Xingguang Wei, Hongjie Zhang, Haomin Wang, Weiyue Xu, Hao Li, Jiahao Wang, Nianchen Deng, Songze Li, Yinan He, Tan Jiang, Jiapeng Luo, Yi Wang, Conghui He, Botian Shi, Xingcheng Zhang, Wenqi Shao, Junjun He, Yingtong Xiong, Wenwen Qu, Peng Sun, Penglong Jiao, Han Lv, Lijun Wu, Kaipeng Zhang, Huipeng Deng, Jiaye Ge, Kai Chen, Limin Wang, Min Dou, Lewei Lu, Xizhou Zhu, Tong Lu, Dahua Lin, Yu Qiao, Jifeng Dai, and Wenhai Wang. Internvl3: Exploring advanced training and test-time recipes for open-source multimodal models, 2025. 1

[67] Younan Zhu, Linwei Tao, Minjing Dong, and Chang Xu. Mitigating object hallucinations in large vision-language models via attention calibration, 2025. 1

[68] Xin Zou, Yizhou Wang, Yibo Yan, Yuanhuiyi Lyu, Kening Zheng, Sirui Huang, Junkai Chen, Peijie Jiang, Jia Liu, Chang Tang, and Xuming Hu. Look twice before you answer: Memory-space visual retracing for hallucination mitigation in multimodal large language models, 2025. 2, 5, 6, 7, 8

Residual Decoding: Mitigating Hallucinations in Large Vision-Language Models via History-Aware Residual Guidance

Supplementary Material

A. Implementation Details

A.1. Datasets

MME [14] evaluates the capabilities of MLLMs, dividing the evaluation into two major categories: perception and cognition. The perception category includes fine-grained tasks such as existence, count, location, rough color, poster, celebrity, scene, landmark, artwork identification, and OCR. The cognition category includes tasks like commonsense reasoning, numerical calculations, text translation, and code reasoning. All questions in this benchmark are structured to be answered with a simple yes or no.

POPE [30] is a metric based on Visual Question Answering (VQA) designed to evaluate hallucinations in MLLMs. This metric assesses the model’s response to the question, “Is [object] in this image?” To clarify that this is a binary VQA task, the prompt is supplemented with the instruction, “Please answer yes or no.” POPE is built on three core data sources: COCO, A-OKVQA, and GQA. We report the overall accuracy and F1-score.

CHAIR [47] is used to assess the alignment between generated captions and the content of the given image. The CHAIR metric consists of two evaluation types: per-instance evaluation (CHAIR_I) and per-sentence evaluation (CHAIR_S), which are defined as follows:

$$\text{CHAIR}_i = \frac{|\{\text{hallucinated objects}\}|}{|\{\text{all objects mentioned}\}|} \quad (11)$$

$$\text{CHAIR}_s = \frac{|\{\text{sentences with hallucinated object}\}|}{|\{\text{all sentences}\}|} \quad (12)$$

HallusionBench [18]. HallusionBench is a benchmark constructed to evaluate hallucination robustness of large vision–language models under challenging, misleading scenarios. It contains 951 carefully curated question–answer pairs, where each question is designed to probe whether a model can resist visually or semantically deceptive cues and avoid generating hallucinated content. This benchmark thus provides a focused testbed for analyzing and improving the reliability of multimodal reasoning.

MMBench [41] is a comprehensive benchmark for evaluating general purpose vision language models. It contains

carefully curated multiple choice questions in both English and Chinese that test perception, reasoning, and understanding across diverse real world images and scenarios.

ScienceQA [42] is a multimodal multiple-choice benchmark that evaluates scientific reasoning over grade-school curricula, with questions accompanied by textual context and often images or diagrams. In our experiments, we adopt the official ScienceQA test split, which consists of 2,017 question–answer pairs, and use it to assess the model’s ability to perform multimodal reasoning and science knowledge understanding.

MMStar [7] is a comprehensive benchmark for evaluating large vision–language models, consisting of 1,500 carefully curated multiple-choice questions that cover a wide range of real-world images and tasks. It is designed to probe fine-grained multimodal abilities, including perception, reasoning, and instruction following, thereby enabling more reliable and nuanced assessment of general-purpose multimodal models.

SEEDBench2_Plus [28] is a large scale benchmark for evaluating multimodal large language models. It contains 2,277 question–answer pairs covering diverse perception and reasoning skills, and provides a fine grained assessment of both visual understanding and high level multimodal reasoning.

MM-Vet [58] is a benchmark designed to assess large vision–language models on challenging, multi-step tasks. It specifies six core capabilities in the vision–language setting: recognition, optical character recognition, factual and commonsense knowledge, language generation, spatial understanding, and mathematical reasoning. To obtain consistent and reliable scores across heterogeneous question formats, it employs a language model as an automatic evaluator. The benchmark contains 187 images collected from diverse online sources and 205 questions, each constructed so that answering it requires one or more of the defined capabilities.

MMVP. MMVP [53] is a benchmark targeting the fine-grained visual recognition ability of LVLMs based on CLIP-blind image pairs. It contains 150 pairs of images, with each pair accompanied by a binary-choice question.

The two images in a pair are evaluated independently, and an LVLM receives credit for a pair only if it answers the questions for both images correctly.

LLaVA-Bench. LLaVA-Bench (In-the-Wild) [38] consists of 24 images representing various complex scenes, memes, paintings, and sketches, paired with 60 challenging questions. A subset of this dataset is used for qualitative comparisons of responses generated by different decoding strategies. we assess the accuracy and depth of the generated responses using GPT-4V.

B. Theoretical Analysis of ResDec

B.1. Derivation of Language Priors

Following Lin et al. [35], we define the *language prior* as the text-only, vision-agnostic conditional distribution $P(y | x)$, which represents the generative tendency of the output sequence $y = (y_1, \dots, y_T)$ given only the textual context x , without considering the visual input v . This language prior is related to the joint distribution of text and vision via the equivalent factorizations:

$$P(y, v | x) = P(y | x) P(v | y, x) = P(v | x) P(y | v, x), \quad (13)$$

where $P(y | x)$ isolates the language-driven preference over the outputs once the visual evidence v is removed. These factorizations highlight how the text-only distribution and visual context interact to form the complete generative process. At the token level, both the visual-conditional likelihood $P(y | v, x)$ and the language prior $P(y | x)$ admit autoregressive factorizations, meaning that the probability of the entire sequence is factorized into the product of the probabilities of each individual token conditioned on the previous ones:

$$\begin{aligned} P(y | v, x) &= \prod_{t=1}^T P(y_t | y_{<t}, v, x), \\ P(y | x) &= \prod_{t=1}^T P(y_t | y_{<t}, x), \end{aligned} \quad (14)$$

The first equation represents the likelihood of the output sequence given both the visual and textual context, while the second equation shows the likelihood given only the textual context. These factorizations treat each token in the sequence independently, conditioned on all previous tokens, allowing for sequential prediction. To compare the visual-conditional likelihood and the language prior, we combine the joint factorizations with Bayes' rule. This results in a ratio that isolates the effect of the visual input relative to the language prior:

Models	Historical Window W	POPE		MME
		Accuracy \uparrow	F1 \uparrow	Accuracy \uparrow
LLaVA-1.5	2	87.05	86.59	1869.23
	4	84.45	82.71	1762.76
	8	87.23	86.93	1881.57
	16	86.96	86.32	1882.41
	32	87.35	87.03	1880.86
Qwen2.5-VL	2	84.33	85.21	2232.54
	4	86.86	85.63	2326.93
	8	90.16	89.56	2348.40
	16	90.33	89.96	2350.52
	32	89.98	89.73	2346.81

Table 7. Performance of predefined historical window W on LLaVA-1.5/Qwen2.5-VL for POPE and MME benchmarks.

$$\frac{P(y | v, x)}{P(y | x)} = \frac{P(y, v | x)}{P(y | x) P(v | x)} = \frac{P(v | y, x)}{P(v | x)}, \quad (15)$$

This ratio quantifies how much the visual input v contributes to the generation process beyond the language prior $P(y | x)$. The ratio serves as a *PMI-style* measure of the influence of the visual context. Taking the logarithm of this ratio turns it into a token-wise subtraction between the visual-conditional and the text-only next-token scores at each timestep t :

$$\log \frac{P(y | v, x)}{P(y | x)} = \sum_{t=1}^T \left[\log P(y_t | y_{<t}, v, x) - \log P(y_t | y_{<t}, x) \right], \quad (16)$$

This formulation allows us to evaluate how much the visual context adjusts the prediction for each token, removing the contribution of the language prior. Finally, the language prior itself can be expressed as a marginalization over the visual variable v , which accounts for all possible visual contexts. This marginalization is given by:

$$P(y | x) = \mathbb{E}_{v \sim P(v|x)}[P(y | v, x)], \quad (17)$$

where the expectation is taken over all possible visual inputs v , conditioned on the textual context x . In practice, this expectation is approximated using Monte Carlo sampling, which gives:

$$P(y | x) \approx \frac{1}{n} \sum_{j=1}^n P(y | v_j, x), \quad (18)$$

where $\{v_j\}_{j=1}^n$ are samples drawn from the image distribution conditioned on x . This Monte Carlo approximation effectively captures the language prior while accounting for the variability in the visual context.

B.2. Theoretical Analysis

Definitions. Let V be the visual variable, H the history (image tokens + past text), and Y the next-token output. Denote the baseline decoder by $p(y | v, h)$ and the residual-induced distribution by $r(y | v, h)$. ResDec forms the α -blended channel

$$p_\alpha(y | v, h) := \frac{p(y | v, h)^{1-\alpha} r(y | v, h)^\alpha}{Z_\alpha(v, h)},$$

$$Z_\alpha(v, h) := \sum_{y'} p(y' | v, h)^{1-\alpha} r(y' | v, h)^\alpha.$$

Write the H -marginal as

$$p_\alpha(y | h) := \sum_v p_\alpha(y | v, h) p(v | h).$$

The conditional mutual information is

$$I_\alpha(V; Y | H) := \mathbb{E}_h [\text{KL}(p_\alpha(\cdot | v, h) \| p_\alpha(\cdot | h))].$$

Define the *residual advantage*

$$A(y, v, h) := \log r(y | v, h) - \log r(y | h).$$

Theorem 1. Assume regularity so that differentiation under the expectation is valid, and suppose the residual is informative in the sense that for some $\varepsilon > 0$,

$$\mathbb{E}_h \mathbb{E}_{v|h} \mathbb{E}_{y \sim p(\cdot | v, h)} [A(y, v, h)] \geq \varepsilon.$$

Then the directional derivative of the conditional MI at $\alpha = 0$ satisfies

$$\frac{d}{d\alpha} I_\alpha(V; Y | H) \Big|_{\alpha=0} = \mathbb{E}_h \mathbb{E}_{v|h} \mathbb{E}_{y \sim p(\cdot | v, h)} [A(y, v, h)] \geq \varepsilon.$$

Consequently, there exists $\alpha_0 > 0$ such that for all $\alpha \in (0, \alpha_0]$,

$$I_\alpha(V; Y | H) \geq I_0(V; Y | H) + \frac{\varepsilon}{2} \alpha.$$

Proof. Rewrite p_α as an exponential tilt of p :

$$p_\alpha(y | v, h) = \frac{p(y | v, h) \exp(\alpha U_v(y))}{Z_\alpha(v, h)},$$

$$U_v(y) := \log r(y | v, h) - \log p(y | v, h).$$

Similarly,

$$p_\alpha(y | h) = \frac{p(y | h) \exp(\alpha \bar{U}(y))}{\bar{Z}_\alpha(h)},$$

$$\bar{U}(y) := \log r(y | h) - \log p(y | h).$$

For the log-densities, exponential-family calculus gives

$$\frac{\partial}{\partial \alpha} \log p_\alpha(y | v, h) \Big|_0 = U_v(y) - \mathbb{E}_{y' \sim p(\cdot | v, h)} [U_v(y')],$$

$$\frac{\partial}{\partial \alpha} \log p_\alpha(y | h) \Big|_0 = \bar{U}(y) - \mathbb{E}_{y' \sim p(\cdot | h)} [\bar{U}(y')].$$

Differentiating the KL form of I_α at $\alpha = 0$ and using $\frac{d}{d\alpha} \text{KL}(P_\alpha \| Q_\alpha) = \mathbb{E}_{P_\alpha} [\partial_\alpha \log P_\alpha - \partial_\alpha \log Q_\alpha]$ at $\alpha = 0$ yields

$$\frac{d}{d\alpha} I_\alpha \Big|_0 = \mathbb{E}_h \mathbb{E}_{v|h} \mathbb{E}_{y \sim p(\cdot | v, h)} [(U_v(y) - \bar{U}(y))].$$

With the definitions of U_v and \bar{U} , the bracket equals

$$\begin{aligned} & (\log r(y | v, h) - \log p(y | v, h)) \\ & - (\log r(y | h) - \log p(y | h)) \\ & = A(y, v, h) - \text{PMI}_p(y; v | h). \end{aligned}$$

Taking expectation over $y \sim p(\cdot | v, h)$ cancels the PMI_p term, giving the stated derivative. The claimed local increase follows by continuity.

Theorem 2. Let v be the visual input, x the text query, and h the decoding history. Denote the base logits by $\ell(y | v, x, h)$ and the residual offsets by $r_h(y)$. Define the base and residual-augmented conditional distributions

$$p_0(y | v, x, h) = \text{softmax}(\ell(y | v, x, h)),$$

$$p_\alpha(y | v, x, h) = \text{softmax}(\ell(y | v, x, h) + \alpha r_h(y)),$$

with $\alpha \in (0, 1]$. Equivalently,

$$p_\alpha(y | v, x, h) = \frac{p_0(y | v, x, h) \exp(\alpha r_h(y))}{Z(\alpha)},$$

$$Z(\alpha) = \sum_{y'} p_0(y' | v, x, h) \exp(\alpha r_h(y')).$$

Assume the residual aligns with the desirable visual grounding in the sense that $\text{Cov}_{p_\alpha}(r_h(Y), \log p_0(Y | v, x, h)) \geq 0$ for $\alpha \in [0, 1]$, and $\text{Var}_{p_\alpha}(r_h(Y)) > 0$. Then, for any $\alpha \in (0, 1]$, the conditional Shannon entropy strictly decreases:

$$H(Y | v, x, h)_{p_\alpha} < H(Y | v, x, h)_{p_0}.$$

Proof. Use the exponential-tilted form of p_α displayed above and write the conditional entropy under p_α as

$$\begin{aligned} H_\alpha &= - \sum_y p_\alpha(y) \log p_\alpha(y) \\ &= -\mathbb{E}_{p_\alpha} [\log p_0(Y)] - \alpha \mathbb{E}_{p_\alpha} [r_h(Y)] + \log Z(\alpha). \end{aligned}$$

Differentiate with respect to α . Invoking the standard score function identity for the α -indexed family $\{p_\alpha\}$, namely $\frac{d}{d\alpha} \mathbb{E}_{Y \sim p_\alpha} [f(Y)] = \text{Cov}_{Y \sim p_\alpha} (f(Y), r_h(Y))$ for any integrable test function f , and using $\frac{d}{d\alpha} \log Z(\alpha) = \mathbb{E}_{Y \sim p_\alpha} [r_h(Y)]$, we obtain

$$\begin{aligned} \frac{d}{d\alpha} H_\alpha &= -\text{Cov}_{p_\alpha} (\log p_0(Y), r_h(Y)) - \mathbb{E}_{p_\alpha} [r_h(Y)] \\ &\quad - \alpha \text{Cov}_{p_\alpha} (r_h(Y), r_h(Y)) + \mathbb{E}_{p_\alpha} [r_h(Y)]. \end{aligned}$$

The middle expectations cancel, yielding

$$\frac{d}{d\alpha} H_\alpha = - \text{Cov}_{p_\alpha}(\log p_0(Y), r_h(Y)) - \alpha \text{Var}_{p_\alpha}(r_h(Y)).$$

Under the alignment assumption, $r_h(Y)$ is positively associated with the base log-likelihood $\log p_0(Y)$, hence $\text{Cov}_{p_\alpha}(\log p_0(Y), r_h(Y)) \geq 0$. Moreover, the residual signal is non-degenerate under p_α , so $\text{Var}_{p_\alpha}(r_h(Y)) > 0$. These conditions hold for all α and together capture positive association with nontrivial variability; therefore, for any $\alpha > 0$,

$$\frac{d}{d\alpha} H_\alpha < 0.$$

Integrating from 0 to any $\alpha \in (0, 1]$ gives

$$H_\alpha - H_0 = \int_0^\alpha \frac{d}{ds} H_s ds < 0,$$

which is precisely the claimed entropy decrease.

C. Predefined Historical Window

In this section, we conduct experiments on the Predefined Historical Window W . Since W merely serves as a parameter for identifying the U-shape, we set W to 2, 4, 8, 16, and 32. The corresponding experimental results are presented in Table 7. We find that the U-shape is typically achievable when $W = 8$; thus, we usually set $W = 8$ in our experiments.

D. More Case Studies

Additional case studies are presented to illustrate the effectiveness of our *ResDec*.

[Instruction] Please describe this image in detail.

[Regular Decoding] The image features a green park bench with a bottle of water placed on it. The bench is located near a sidewalk, and there are several people walking by. In the background, a car can be seen parked on the street. There are three people in the scene, with one person walking closer to the left side of the bench, another person walking further to the right, and the third person walking behind the bench. Additionally, there is a **handbag placed on the ground** near the person walking on the left side of the bench.



[Residual Decoding] The image features a green bench in a park, with a blue bottle sitting on the bench, close to the back and the right side. The bench is positioned near a sidewalk, and a street with parked cars can be seen in the background. There are a few people in the scene, with one person standing close to the left side of the bench and, in the background, two more people, one near the left and the other near the right side of the park.

[Instruction] Please describe this image in detail.

[Regular Decoding] The image features a cozy dining room with a dining table set for a meal. The table is adorned with several wine glasses, cups, and a **bottle of wine**. There are also a couple of forks and knives placed on the table. The dining area is furnished with a couch and a chair, providing a comfortable atmosphere for guests to enjoy their meal. The room is decorated with a fireplace, adding warmth and ambiance to the space. **A clock is mounted on the wall**, and a **vase can be seen on the table**, adding to the room's decor. The dining table is surrounded by chairs, and a couch is situated nearby, creating a welcoming and inviting environment for guests to relax and dine.



[Residual Decoding] The image showcases a beautifully decorated dining room, furnished with a dining table and a set of chairs. The table is set with dishes, plates, and wine glasses, ready for a meal. The dining table, with a tablecloth, and chairs surround it, and the setting is inviting and elegant. There are several wine glasses and cups on the table, and a bottle, possibly a wine bottle, is placed on the table as well. The dining table, with a well-arranged set, and the chairs set for a meal, create a cozy and inviting atmosphere for a dining experience.

[Instruction] Please describe this image in detail.

[Regular Decoding] The image features a large, beautifully decorated cake with white frosting and red lettering. The cake is placed on a dining table, and it is adorned with a knife and a **fork**, ready to be cut and served. The cake is **shaped like a heart** and is likely meant to celebrate a special occasion or event. The red lettering on the cake reads "welcome malachi," indicating that it is a welcoming gesture for someone named Malachi.



[Residual Decoding] The image showcases a large cake decorated beautifully, with a red frosting and white frosting to celebrate a welcoming. The cake is topped with a red cake knife, and a decorative cake topper, a red cake topper, and a red cake topper with a cake decor to decorate the cake. The cake is placed on a dining table, and a cake serving spatula is also visible on the table, ready to be used to cut and serve the cake.

[Instruction] Please describe this image in detail.

[Instruction] Please describe this image in detail.

[Regular Decoding] The image features a man standing on the back of a boat, painting a crab on the side of the vessel. The boat is white and blue, and it appears to be a fishing boat. There are several other people on the boat, **some of them standing near the man painting the crab**, while **others are scattered around the boat**. In addition to the people on the boat, there are a few objects visible in the scene. **A bottle can be seen on the boat**, and **a cup is placed nearby**. The presence of these items suggests that the people on the boat might be enjoying a leisurely time together.



[Residual Decoding] The image depicts a man on a boat painted with a crab on the side, a crab painted on the boat. The man is standing on the boat, painting the crab on the side, while a crab painted on the boat nearby. There are several other people on the boat, and a smaller boat can be seen in the background. The boat, with the crab painted on it, is the main focus of the scene, and the man painting the crab on the side is the most prominent figure in the image.

[Instruction] Please describe this image in detail.

[Instruction] Please describe this image in detail.

[Regular Decoding] The image features a small bathroom with a white toilet and a urinal mounted on the wall. The toilet is positioned on the left side of the bathroom, while the urinal is located on the right side. **The toilet seat is up, revealing the toilet bowl**. There are two toilet paper holders in the bathroom, one on the left side and the other on the right side. **The toilet paper on the left side is placed on the holder**, while the toilet paper on the right side is hanging from the holder. The bathroom appears to be clean and well-maintained.



[Residual Decoding] The image showcases a bathroom stall with a toilet and a urinal, both white in color. The toilet and urinal are positioned close to each other, with the urinal to the right of the toilet. A toilet paper dispenser is mounted on the wall above the toilet, and a toilet paper roll is hanging on the dispenser. The toilet paper dispenser is also next to the urinal to the right of the toilet. In addition to the toilet and urinal, the bathroom stall features a sink, and a toilet paper dispenser is also mounted on the wall above the sink.

[Regular Decoding] The image features a man shearing a sheep in a barn. The man is standing next to the sheep, which is lying on the ground, and he is using a pair of shears to remove the wool. The sheep appears to be a large, fluffy animal, and the man is focused on his task. In the background, **there are two other sheep, one on the left side and another on the right side of the image**. Additionally, **there are two people present in the scene**, one standing near the left side of the image and another person standing near the right side. **A bottle can also be seen on the ground**, possibly containing a shearing tool or a cleaning solution.



[Residual Decoding] The image depicts a man shearing a sheep in a sheep shearing shed. The sheep is on the ground, and the man is shearing the wool with shears in his hands. The shearing process is in progress, and the man is focused on the task. There are several other sheep in the background, and a nearby fence can be seen, enclosing the area. The man and the sheep in the foreground are the main focus of the scene, showcasing the shearing process in action.

Figure 6. More examples comparing regular decoding and residual decoding in image captioning. Hallucinated details in “regular” decoding outputs are highlighted in red.



[Question] Is there a baseball bat in the image?

LLaVA-1.5 [Regular Decoding] Yes.

LLaVA-1.5 [Residual Decoding] No.



[Question] Is there a bicycle in the image?

LLaVA-1.5 [Regular Decoding] No.

LLaVA-1.5 [Residual Decoding] Yes.



[Question] Is there a wine glass in the image?

LLaVA-1.5 [Regular Decoding] Yes.

LLaVA-1.5 [Residual Decoding] No.



[Question] Is there a bottle in the image?

LLaVA-1.5 [Regular Decoding] No.

LLaVA-1.5 [Residual Decoding] Yes



[Question] Is there a stop sign in the image?

LLaVA-1.5 [Regular Decoding] Yes.

LLaVA-1.5 [Residual Decoding] No.



[Question] Is there a stop sign in the image?

LLaVA-1.5 [Regular Decoding] Yes.

LLaVA-1.5 [Residual Decoding] No.

Figure 7. More examples comparing regular decoding and residual decoding in image captioning. Hallucinated details in “regular” decoding outputs are highlighted in red.



[Question] Is there a toothbrush in the image?

Qwen2.5-VL [Regular Decoding] No.

Qwen2.5-VL [Residual Decoding] Yes.



[Question] Is there a mouse in the image?

Qwen2.5-VL [Regular Decoding] No.

Qwen2.5-VL [Residual Decoding] Yes.



[Question] Is there a bowl in the image?

Qwen2.5-VL [Regular Decoding] Yes.

Qwen2.5-VL [Residual Decoding] No.



[Question] Is there a truck in the image?

Qwen2.5-VL [Regular Decoding] No.

Qwen2.5-VL [Residual Decoding] Yes.



[Question] Is there a backpack in the image?

Qwen2.5-VL [Regular Decoding] No.

Qwen2.5-VL [Residual Decoding] Yes.



[Question] Is there a bench in the image?

Qwen2.5-VL [Regular Decoding] Yes.

Qwen2.5-VL [Residual Decoding] No.

Figure 8. More examples comparing regular decoding and residual decoding in image captioning. Hallucinated details in “regular” decoding outputs are highlighted in red.